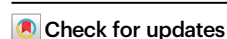


Neoadjuvant Aumolertinib for unresectable stage III *EGFR*-mutant non-small cell lung cancer: a single-arm phase II trial

Received: 21 August 2024

Accepted: 21 March 2025

Published online: 02 April 2025



A list of authors and their affiliations appears at the end of the paper

Aumolertinib, a third-generation epidermal growth factor receptor tyrosine kinase inhibitor (*EGFR*-TKI), is widely utilized for advanced *EGFR*-mutant non-small cell lung cancer patients (NSCLCm). This single-arm, phase II trial (NCT04685070) assessed the feasibility of neoadjuvant Aumolertinib for unresectable stage III NSCLCm. Fifty-six patients were enrolled, with 51 participants receiving neoadjuvant Aumolertinib (110 mg/day, orally) and forming the intention-to-treat population. The primary endpoint was objective response rate (ORR). Secondary endpoints included major pathological response (MPR) rate, pathological complete response (pCR) rate, complete (R0) resection rate, event-free survival (EFS), overall survival (OS), and treatment-related adverse events (TRAEs). The ORR was 70.6% (95% confidence interval: 58%–84%), meeting the pre-specified primary endpoint. Additionally, twenty-three (45.1%) participants converted into resectable disease and underwent surgery. Among them, R0 resection, MPR and pCR rates were 100%, 21.7%, and 13.0%, respectively. The median EFS and OS were not reached. While, the 1- and 2-year EFS rates were 88.2% and 58.8%, respectively. Fatigue (49.0%), alanine aminotransferase concentration elevation (39.2%), and rash (35.3%) were the most common treatment-related adverse events (TRAEs). Grade 3/4 TRAEs occurred in 5 patients (9.8%), and no grade 5 TRAE was recorded. RNA-sequencing based analysis revealed increased infiltration of CD8 + T-cells in post-treatment tumors compared to baseline, particularly in responsive and Ex19-Del mutation tumors. Collectively, neoadjuvant Aumolertinib showed promising efficacy and a surgical conversion rate with a tolerable safety profile for unresectable NSCLCm in stage III, potentially involved in the remodeling of tumor microenvironment.

Lung cancer has the highest incidence among malignant tumors worldwide, with non-small cell lung cancer (NSCLC) accounting for approximately 85% of cases¹. Over 15% of NSCLC patients are diagnosed as stage III (according to the 8th edition lung cancer TNM staging system), and most of these cases are considered unresectable². The epidermal growth factor receptor (*EGFR*) is one of the most common driver oncogenes in NSCLC, with a prevalence of 50% among Chinese patients³.

The latest National Comprehensive Cancer Network (NCCN) guideline recommended that Durvalumab (anti-PD-L1 antibody) after concurrent chemoradiotherapy (cCRT) (PACIFIC regimen) could be performed for unresectable stage III NSCLC harboring *EGFR* mutation (NSCLCm)⁴. Additionally, GEMSTONE-301 study⁵ demonstrated that, Sugemalimab (anti-PD-L1 antibody) may confer a prognostic benefit for patients with unresectable stage III NSCLC when administered following concurrent

✉ e-mail: wuchunyan581@163.com; zdp1992@163.com; duan-liang@163.com; geningjiang@tongji.edu.cn; zhangpeng1121@tongji.edu.cn

or sequential chemoradiotherapy (cCRT/sCRT). However, over 80% of patients treated with the PACIFIC regimen relapse within 5 years, primarily due to distant metastasis^{4,6}. Therefore, there is an urgent need to update the treatment regimen for unresectable NSCLCm in stage III.

Third-generation *EGFR* tyrosine kinase inhibitors (*EGFR*-TKIs) are recommended as the first-line treatment for advanced NSCLCm⁷. Additionally, Osimertinib (a third-generation *EGFR*-TKI) has been recommended as maintenance therapy after chemoradiotherapy and surgery for inoperable stage III NSCLCm (as seen in the LAURA trial) and operable stage III NSCLCm, respectively (as seen in the ADAURA trial)^{8,9}. However, the feasibility of neoadjuvant *EGFR*-TKIs followed by radical surgery for stage III NSCLCm still requires further data from prospective clinical trials^{10–14}. Our previous single-arm phase II study (TEAM-LungMate 004) demonstrated that neoadjuvant Afatinib (a second-generation *EGFR*-TKI) could convert 56% of unresectable stage III NSCLCm into a resectable state, offering a relatively favorable prognosis. This finding supports the feasibility of neoadjuvant target-therapy combined with radical surgery for initially unresectable stage III NSCLCm¹¹.

Aumolertinib (formerly known as HS-10296 or Almonertinib) is a third-generation *EGFR*-TKI with highly selectivity for *EGFR*-sensitizing and exon 20 codon p.Thr790Met point mutation (T790M)¹⁵. In 2022, Aumolertinib monotherapy was approved in China for the first-line treatment of NSCLCm, based on the results of the randomized phase III trial (AENEAS)⁷. This suggests that neoadjuvant Aumolertinib treatment might offer advantages over the PACIFIC regimen for unresectable NSCLCm in stage III. However, there are limited studies on the efficacy and safety of neoadjuvant Aumolertinib for unresectable stage III NSCLCm^{16,17}.

This single-arm, open-label, phase II clinical trial (LungMate 007, NCT04685070) aims to assess the efficacy and safety of neoadjuvant Aumolertinib for unresectable stage III NSCLCm. This trial successfully achieved the pre-specified primary endpoint, with an objective response rate (ORR) of 70.6%, which was higher than the ORR expected at the time of trial design (70.0%).

Results

Baseline characteristics

Between December 2021 and June 2023, a total of 56 unresectable NSCLCm patients in stage III were enrolled in this trial (Fig. 1). Among

them, 5 patients withdrew their informed consents, leaving 51 participants who received neoadjuvant Aumolertinib treatment as the intention-to-treat (ITT) population, as detailed in Table 1. The average diagnostic age was 62.6 years (range, 40–76 years), with a majority of participants being female (28/51, 54.9%), never-smokers (35/51, 68.6%), and having an ECOG performance status of 0 (30/51, 58.8%). Within the ITT population, 22 participants (43.1%) had the Ex19-Del mutation, while 27 (52.9%) had the Ex21-L858R mutation. There were 2 participants harboring uncommon *EGFR* mutations (Supplementary Table 1). Most participants were categorized as having stage N2 disease (25/51, 49.0%). The distribution of disease stages included 24 participants (47.1%) with stage IIIA, 22 (43.1%) with stage IIIB, and 5 (9.8%) with stage IIIC. The mean maximum target-lesions dimension (TLD) on CT was 50.0 mm (range, 17–113 mm) and the mean maximum standardized uptake value (SUVmax) for glucose metabolism of the primary tumor on PET-CT was 11.7 (range, 3.5–26.8).

Efficacy

The efficacy of neoadjuvant Aumolertinib treatment was demonstrated in Table 2. After a median of 4 cycles (range, 2–6 cycles) of neoadjuvant treatment, ORR, the primary endpoint, was 70.6% (95% CI: 58–84%). The disease control rate (DCR) was 100%. The waterfall plots illustrating the responses were shown in Fig. 2a.

For the secondary endpoints, 23 participants proceeded from neoadjuvant treatment to radical surgery, resulting in a surgical conversion rate of 45.1% (23/51). All participants who underwent surgery achieved complete (R0) resection. The major pathological response (MPR) was assessed in these cases (Fig. 2b). Among five participants who achieved MPR (MPR rate: 21.7%, 95% CI: 4–40%), three participants achieved pathologic complete response (pCR) (pCR rate: 13.0%, 95% CI: 2–28%). Additionally, the mean percentage of residual tumor cells in the primary tumor was 45.9% (range, 0% to 100%). The average duration of postoperative hospital stay was 5.6 days (range, 4 to 14 days). During surgery, the mean operation time was 116.1 min (range, 60 to 242 min), with mean blood loss of 96.5 mL (range, 20 to 1000 mL). All 23 participants who underwent surgery received adjuvant treatment postoperatively, including *EGFR*-TKI monotherapy ($n=20$), platinum-based chemotherapy ($n=2$), and combination of *EGFR*-TKI and chemotherapy ($n=1$). There were 19 (82.6%) patients

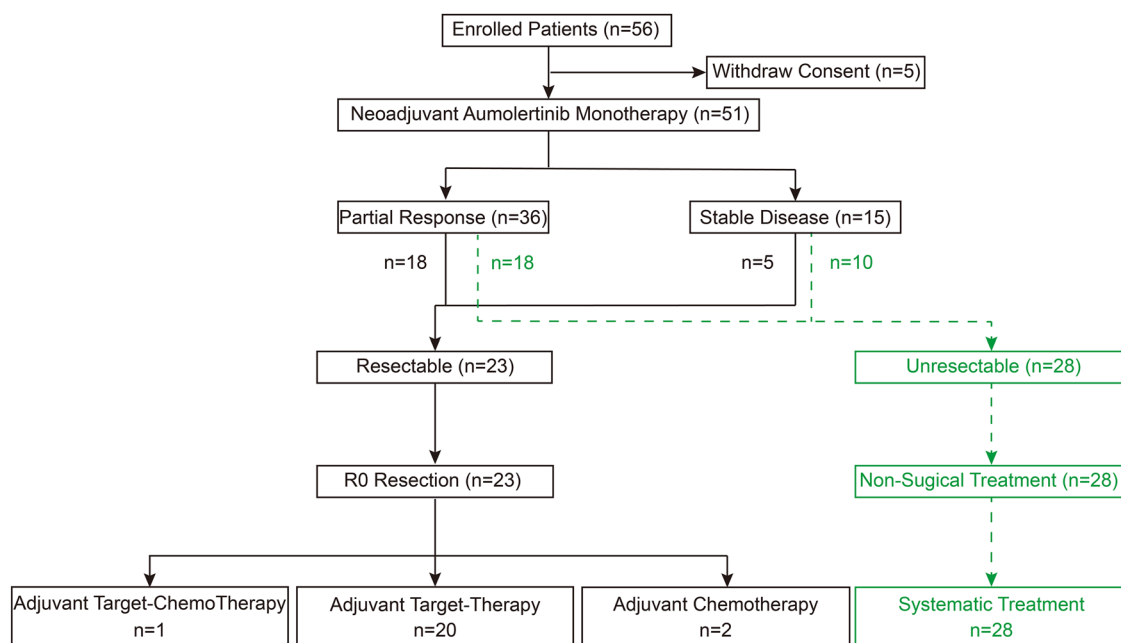


Fig. 1 | The clinical trial (LungMate 007) design.

Table 1 | Baseline characteristics of neoadjuvant Aumolertinin treated patients (n = 51)

Variables	All Patients	Mutant Subtypes, No. (%)		
		Ex19-Del	Ex21-L858R	P
No. of Patients (%)	51	22 (43.1)	27 (56.9)	
Age, years (range)				0.170
	62.6 (40–76)	61.1 (47–75)	64.7 (40–76)	
Gender				0.740
Male	23 (45.1)	10 (45.5)	11 (40.7)	
Female	28 (54.9)	12 (54.5)	16 (59.3)	
ECOG				0.362
0	30 (58.8)	11 (50.0)	17 (63.0)	
1	21 (41.2)	11 (50.0)	10 (37.0)	
Smoking Status				0.869
Ever	16 (31.4)	15 (68.2)	19 (70.4)	
Never	35 (68.6)	7 (31.8)	8 (29.6)	
PD-L1 Expression				0.282
Positive	12 (23.5)	7 (31.8)	5 (18.5)	
Negative or unknow	39 (76.5)	15 (68.2)	22 (81.5)	
TLD in CT, mm (range)				0.055
	50.0 (17–113)	54.1 (20–92)	42.9 (17–111)	
PT-S in PET-CT				0.567
	11.7 (3.5–26.8)	11.2 (3.9–23.4)	12.0 (3.5–26.8)	
N Stage				0.037
1	11 (21.6)	6 (27.3)	5 (18.5)	
2	25 (49.0)	6 (27.3)	17 (63.0)	
3	15 (29.4)	10 (45.4)	5 (18.5)	
cTNM Stage				0.242
IIIA	24 (47.1)	11 (50.0)	13 (48.1)	
IIIB	22 (43.1)	7 (31.8)	13 (48.1)	
IIIC	5 (9.8)	4 (18.2)	1 (3.8)	
Histological Subtype				0.096
Pure LUAD	46 (90.2)	18 (81.8)	26 (96.3)	
NSCLC containing other subtypes	5 (9.8)	4 (18.2)	1 (3.7)	
EGFR Mutation				/
Ex19Del	22 (43.1)	22	0	
L858R	27 (52.9)	0	27	
Uncommon	2 (4.0)	0	0	

LUAD lung adenocarcinoma, NO number, NSCLC non-small cell lung cancer, PT-S maximum standardized uptake value of glucose metabolism of primary tumor, TLD target-lesions dimension.

received adjuvant target-therapy long-term or until the disease progresses.

Sub-group analyses for mutation subtypes

The baseline characteristics between participants with Ex19-Del and Ex21-L858R mutations were demonstrated in Table 1. Participants harboring Ex19-Del had a significantly higher N-stage compared to those who with Ex21-L858R mutation (N3: 45.4% vs 18.5%, $p = 0.037$). In addition, no significant differences were observed in demographic, radiologic, and oncologic characteristics between the two sub-groups.

As shown in Table 2, there was no difference in the number of neoadjuvant treatment cycles between Ex19-Del and Ex21-L858R participants (median treatment cycle: 4 cycles vs 4 cycles, $p = 0.397$). The

Table 2 | Evaluation of efficacy of neoadjuvant Aumolertinin (n = 51)

Variables	All Patients	Mutant Subtypes, No. (%)		
		Ex19-Del	Ex21-L858R	P
Median Neoadjuvant Treatment cycle (range)				0.397
	4.0 (2–6)	4.0 (3–4)	4.0 (3–6)	
Surgery Treatment				0.445
Performed	23	9 (40.9)	14 (51.9)	
Non-Performed	28	13 (50.1)	13 (48.1)	
Tumor Response				0.006
PR	36 (70.6)	20 (90.9)	16 (59.3)	
SD	15 (29.4)	2 (9.1)	11 (40.7)	
ORR (%)				0.362
	70.6	90.9	59.3	
DCR (%)				/
	100.0	100.0	100.0	
TLD Response in CT, % (range)				0.003
	37.8 (–4–86)	45.8 (6–86)	31.2 (0–58)	
PT-S Response in PET-CT, % (range)*				0.557
	64.8 (3.5–100.0)	66.0 (3.0–100.0)	72.3 (7.8–89.7)	
ypN Downstaging [‡]				0.190
	17 (73.9)	8 (88.9)	9 (64.3)	
ypTNM [‡]				0.219
O/I	13 (56.6)	7 (77.8)	6 (42.9)	
II	3 (13.0)	1 (11.1)	2 (14.2)	
III	7 (30.4)	1 (11.1)	6 (42.9)	
Type of Surgery [‡]				/
Thoracotomy	2 (8.7)	2 (22.2)	0 (0.0)	
VATS	21 (91.3)	7 (77.8)	14 (100.0)	
Surgical Resection [‡]				0.106
Lobectomy	19 (82.6)	6 (66.7)	13 (92.9)	
Bi-Lobectomy	4 (17.4)	3 (33.3)	1 (7.1)	
Residual Tumor Cell, % (range) [‡]				0.015
	45.9 (0–100)	19.8 (0–55)	63.3 (5–100)	
Pathologic Regression [‡]				0.034
pCR	3 (13.0)	3 (33.3)	0 (0.0)	
MPR	5 (21.7)	4 (44.4)	1 (7.1)	
Non-MPR	18 (78.3)	5 (55.6)	13 (92.9)	

DCR disease control rate, MPR major pathological response, NO number, ORR objective response rate, pCR pathological complete response, PR partial response, PT-S maximum standardized uptake value of glucose metabolism of primary tumor, SD stable disease, TLD target-lesions dimension.

*Patients received PET-CT before and after neoadjuvant therapy, [‡]Patients received neoadjuvant therapy followed by surgery.

conversion rate of radical surgery was not significantly different between the Ex19-Del group (9/22, 40.9%) and the Ex21-L858R group (14/27, 51.9%). Among those who underwent surgery, participants with Ex19-Del had a significantly higher MPR rate compared to those with Ex21-L858R (44.4% vs 7.1%, $p = 0.034$), and the proportion of residual tumor cell was significantly lower in the Ex19-Del group (19.8% vs 63.5%, $p = 0.015$).

Based on imaging analysis, significant reductions were observed after neoadjuvant treatment in both Ex19-Del and Ex21-L858R

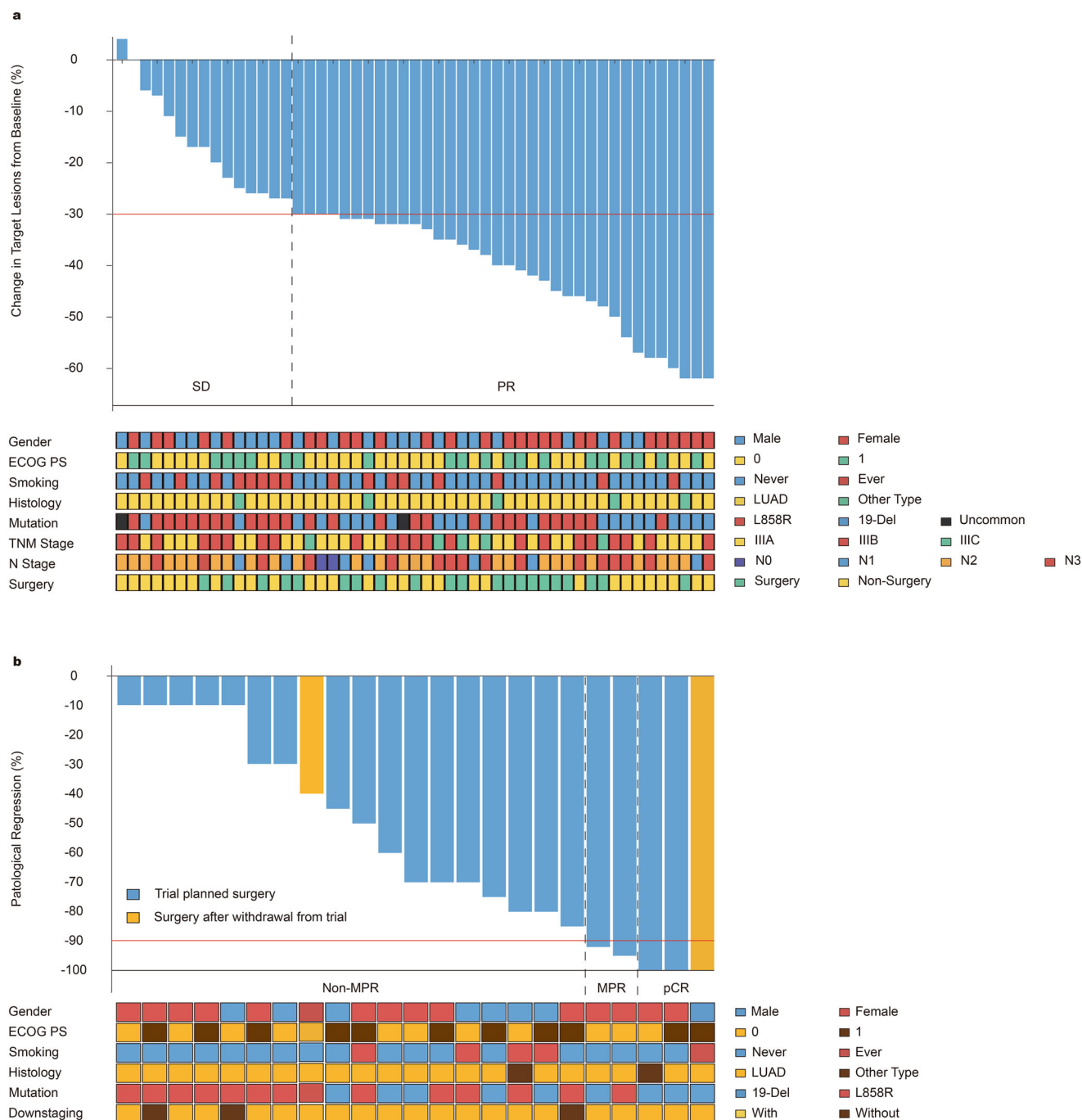


Fig. 2 | Radiological and pathological outcomes of participants. a Waterfall plots of radiological regression of all participants' TLD after neoadjuvant Aumolertinib treatment. **b** Waterfall plots of surgical treated pathological regression. TLD target-

lesions dimension, SD stable disease, PR partial response, MPR major pathological response, pCR complete pathological response. Source data are provided as a Source Data file.

participants. The reductions were noted in target-lesions dimension (TLD) on CT, and primary tumor SUVmax (PT-S) on PET-CT (Fig. 3a, c). Notably, compared with Ex21-L858R participants, those with Ex19-Del exhibited significantly deeper reductions in TLD (TLD: 45.8% vs 31.2%, $p=0.003$; Cohen's d effect size: 1.31 vs 0.76) after neoadjuvant Aumolertinib treatment (Fig. 3b).

Safety

Treatment-related adverse events (TRAEs) are listed in Table 3. Forty-nine participants (96.1%) experienced TRAEs, but no grade 5 TRAEs observed. The most common TRAE of any grade was fatigue, which occurred in 25 (49.0%) of 51 participants. Increases in alanine

aminotransferase concentration (ALT) (20, 39.2%), rash (18, 35.3%), hyponatremia (14, 27.5%), acrodynia (12, 23.5%), stomatitis (11, 21.6%), and thrombocytopenia (11, 21.6%) were also common treatment-related adverse events. Grade 3/4 TRAEs occurred in 5 patients (9.8%), with cases of ALT concentration elevation, aspartate aminotransferase (AST) concentration elevation, pneumonia, thromboembolic event, and ischemia cerebrovascular disease. Discontinuation of Aumolertinib was necessary for two participants due to increased ALT concentration and rash, respectively.

Surgery-related complications were minimal, with one participant experiencing a bronchopleural fistula postoperatively (1/23, 4.3%). No surgery-related death occurred within 90 days postoperatively.

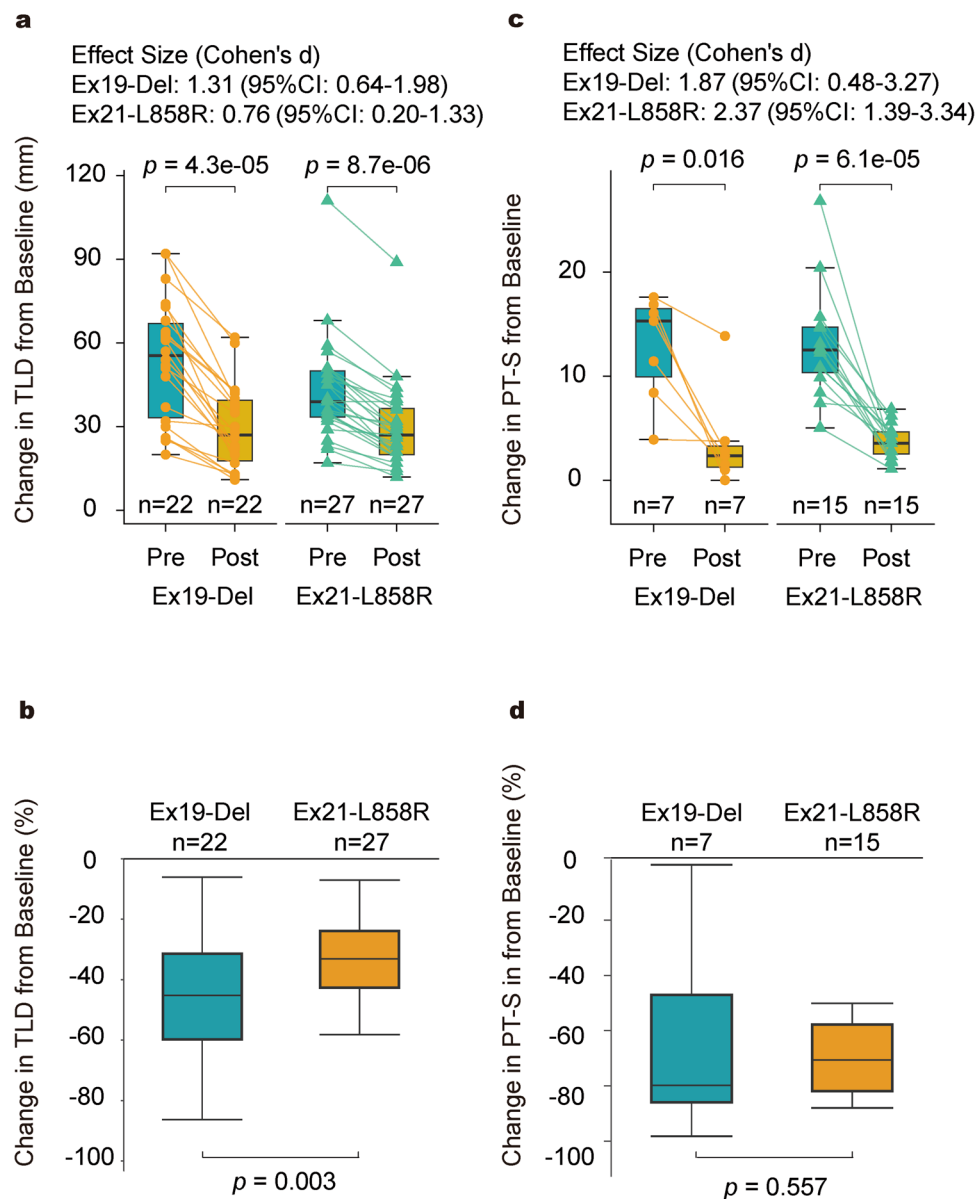


Fig. 3 | Imaging omics for the changing of participants on CT and PET/CT between 2 common mutant subtypes. The trend of radiological changes in (a) TLD via CT (Ex19-Del, $n = 22$; Ex21-L858R, $n = 27$), (c) PT-S via PET-CT (Ex19-Del, $n = 7$; Ex21-L858R, $n = 15$) in paired participants pre- and post-treatment between 2 common mutant subtypes. The degree of radiological changes in (b) TLD via CT (Ex19-Del, $n = 22$; Ex21-L858R, $n = 27$), (d) PT-S via PET-CT (Ex19-Del, $n = 7$; Ex21-L858R, $n = 15$) in participants pre- and post-treatment between 2 common mutant

subtypes. Centers, boxes, whiskers, and dots indicate medians, quantiles, minima/maxima, and outliers, respectively. For difference comparisons in matched samples (a and c), two-sided paired Wilcoxon test was used. For difference comparisons in two independent samples (b and d), two-sided unpaired Wilcoxon test was used. TLD: target-lesions dimension; PT-S: primary tumor SUVmax. Source data are provided as a Source Data file.

Survival analysis

As of the cut-off date of January 1st 2025, the median follow-up duration for all participants was 24.0 months (interquartile range (IQR), 22.0–26.0 months). The median EFS and OS were not reached. The one and two-year EFS rate were 88.2% and 58.8% respectively. Besides, the one and two-year OS rate were 98.0% and 90.2% respectively. Female patients ($p = 0.002$), never smokers ($p = 0.004$), and surgical treated patients ($p = 0.039$) had significantly better EFS. No significant difference in EFS was observed between the participants harboring Ex19-Del and Ex21-L858R ($p = 0.702$). While, EFS of sensitive mutations demonstrated significantly superior than participants with uncommon mutant-subtypes (Ex18-G719X and Ex20-S768I) ($p < 0.001$ for both) (Supplementary Fig. 1).

As the last follow-up, 22 participants experienced events (Supplementary Fig. 2). Of these, seven underwent radical

surgery, with three developing central nervous system (CNS) metastasis postoperatively (42.9%). The remaining 15 participants who experienced events did not receive surgery. Among these, primary tumor progression occurred in 14 participants (93.3%) and CNS metastasis in one participant (6.7%). Additionally, TRAEs led to treatment regimen adjustments in two non-surgery participants.

Exploratory analysis

To explore the molecular characteristics of the tumor microenvironment (TME) during Aumolertinib therapy, we performed bulk RNA-sequencing (RNA-seq) on the primary tumor specimens collected at both baseline and post-treatment phases. After quality control, 23 samples from 23 participants were deemed suitable for downstream analyses (Fig. 4a).

Table 3 | Adverse events in neoadjuvant therapy and surgery

Type of event	No. of Participants		
	Grades 1-4 (%)	Grade 3-4 (%)	SAE (%)
Adverse Event (n = 51)	49 (96.1)	5 (9.8)	4 (7.8)
Fatigue	25 (49.0)	0	0
ALT elevation	20 (39.2)	1 (2.0)	1 (2.0)
Rash	18 (35.3)	0	0
Hyponatremia	14 (27.5)	0	0
Acrodynia	12 (23.5)	0	0
Stomatitis	11 (21.6)	0	0
Thrombocytopenia	11 (21.6)	0	0
AST elevation	10 (19.6)	1 (2.0)	0
Hyperglycemia	8 (15.7)	0	0
Diarrhea	6 (11.8)	0	0
Creatinine elevation	5 (9.8)	0	0
Chest pain	5 (9.8)	0	0
Neutropenia	4 (7.8)	0	0
Blood bilirubin elevation	4 (7.8)	0	0
Stomachache	3 (5.9)	0	0
Anemia	3 (5.9)	0	0
Nausea	3 (5.9)	0	0
Pruritus	3 (5.9)	0	0
Pneumonia	2 (3.9)	1 (2.0)	1 (2.0)
Abdominal pain	2 (3.9)	0	0
Abdominal distension	2 (3.9)	0	0
Headache	2 (3.9)	0	0
Toothache	2 (3.9)	0	0
Lymphopenia	2 (3.9)	0	0
Lightheadedness	2 (3.9)	0	0
Constipation	2 (3.9)	0	0
Hyperuricemia	2 (3.9)	0	0
Thromboembolic event	1 (2.0)	1 (2.0)	1 (2.0)
Ischemia cerebrovascular	1 (2.0)	1 (2.0)	1 (2.0)
Hyperpotassemia	1 (2.0)	0	0
Hypercalcemia	1 (2.0)	0	0
Urinary tract infection	1 (2.0)	0	0
Arrhythmia	1 (2.0)	0	0
Anorexia	1 (2.0)	0	0
Surgical-Related Complications (n = 23)			
Bronchopleural Fistula	1 (4.3)	0	0

ALT alanine aminotransferase, AST aspartate aminotransferase, NO number.

TME remodeling after Aumolertinib treatment in responders

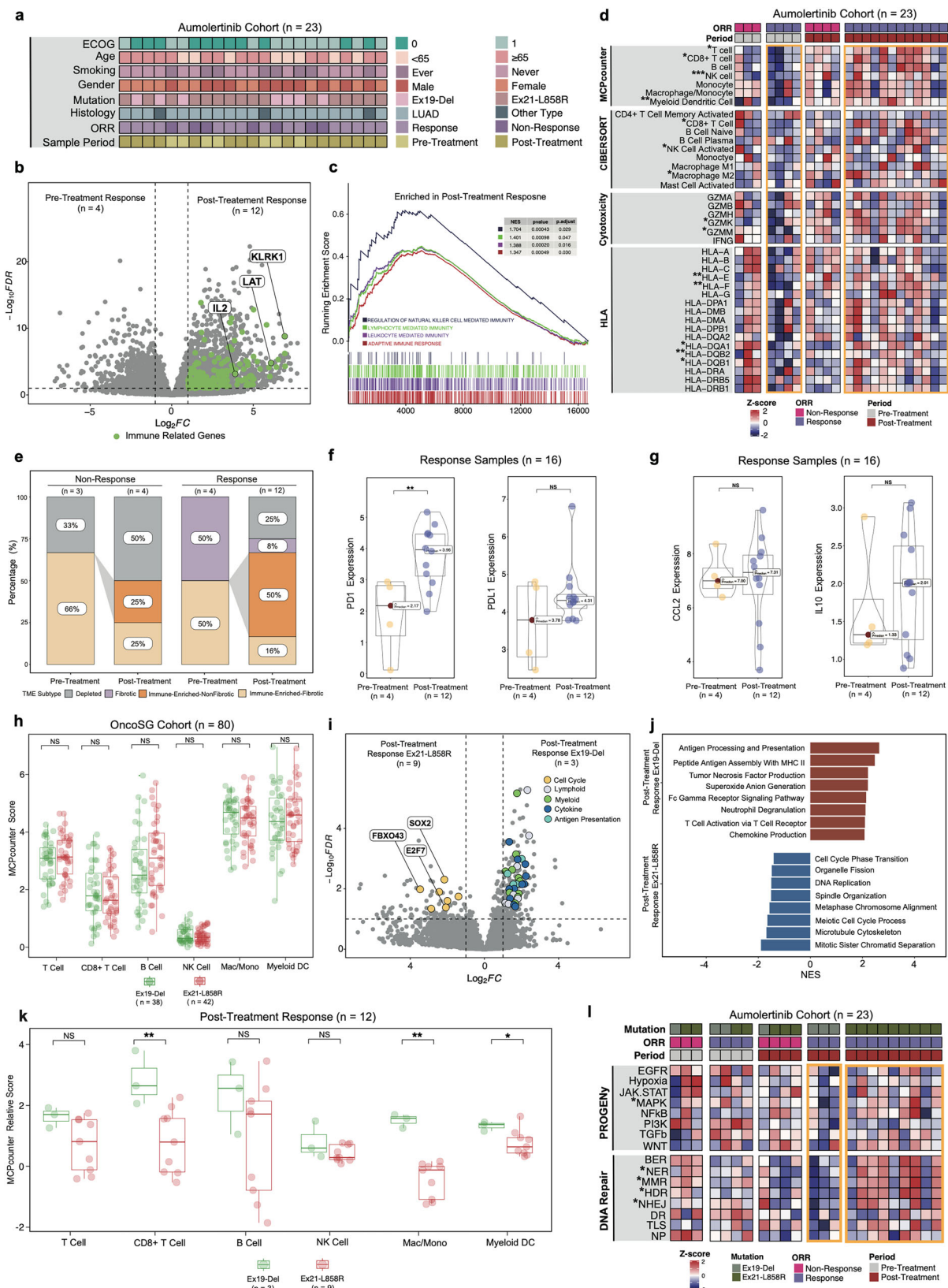
In this trial, TME in non-responders did not show significant changes between baseline and post-treatment phases (Supplementary Fig. 3b, e, f). Consequently, our focus shifted to the dynamics of the TME in responders. Compared to baseline, immune-related genes (such as *IL2*, *LAT*, and *KLRK1*) that are involved in regulating the proliferation and activation of T-cells and NK-cells^{18–20}, were significantly upregulated in post-treatment tumors (Fig. 4b). Gene Set Enrichment Analysis (GSEA) revealed significant enrichment in pathways related to NK cells, lymphocytes, leukocytes, and adaptive immune response in responders after therapy, suggesting potential immune activation due to Aumolertinib treatment (Fig. 4c, Supplementary Fig. 3a). Incidentally, pathways related to “Cell Junction Organization” and “Regulation of Cell Substrate Adhesion” were also found to be downregulated in post-treatment samples (Supplementary Fig. 3b). Immune deconvolution analysis using MCPcounter and CIBERSORT algorithm^{21,22} also

identified an increased infiltration of CD8 + T cells, NK cells, and myeloid dendritic cells following Aumolertinib treatment (Fig. 4d). These findings were partially corroborated by quanTIseq²³ and TIMER²⁴ analyses (Supplementary Fig. 3c). Furthermore, we observed dynamic changes in cytotoxic molecules and HLA during treatment (Fig. 4d). Notably, the post-treatment elevation in cytotoxic molecules and HLA suggested a robust activation of cellular immunity, with a pronounced effect on CD8 + T cells. Although this increase was not statistically significant in non-responsive samples, a similar increasing trend was noted (Supplementary Fig. 3d). Spearman correlation analysis also showed a high correlation among CD8 + T cells, NK cells, and myeloid dendritic cells in post-treatment responsive samples (Supplementary Fig. 3e).

To further delineate the immune ecosystem of post-treatment tumors in responders, we employed the four conserved TME subtypes (depleted, fibrotic, immune-enriched-nonfibrotic, and immune-enriched-fibrotic) proposed by previous studies²⁵ in our cohort (Supplementary Fig. 3f). These results indicated that the immune-enriched-nonfibrotic subtype, theoretically most favorable for immunotherapy, was absent at baseline but emerged after therapy (Fig. 4e). Notably, PD-1 expression was significantly upregulated in tumors after neoadjuvant Aumolertinib treatment compared to baseline, with an increasing trend in PD-L1 expression (Fig. 4f). In non-response samples, similar trends for PD-1 and PD-L1 were not evident (Supplementary Fig. 3g). Additionally, although continuous TKI administration is associated with elevated levels of CCL2 and IL10, which was reported to suppress anti-tumor immunity^{26,27}, similar results were also observed with an increased trend in either the response or non-response groups following neoadjuvant Aumolertinib treatment (Fig. 4g, Supplementary Fig. 3h).

The dynamic differences between Ex19-Del and Ex21-L858R mutations

The participants harboring Ex19-Del mutation had significantly higher responsive rates compared to those with Ex21-L858R mutation (91% vs 59%, $p = 0.006$) after neoadjuvant Aumolertinib treatment (Fig. 2a). This finding prompted an investigation into the differences in the TME between tumors that harbored Ex19-Del mutation and Ex21-L858R mutation. In treatment-naïve tumors (OncoSG cohort)²⁸, there were no significant differences in immune infiltrations between Ex19-Del and Ex21-L858R tumors (Fig. 4h). However, for post-treatment samples, tumors with Ex19-Del mutation exhibited higher expression of immune-related genes compared to those with Ex21-L858R mutation (Fig. 4i). Conversely, cell cycle-related genes (*FBXO43*, *E2F7* and *SOX2*)^{29–32} were up-regulated in tumors with Ex21-L858R mutation (Fig. 4i). Consistent with these observations, GSEA analysis indicated that pathways related to “antigen presentation, cytotoxicity, and tumor necrosis factor production” were significantly upregulated in Ex19-Del samples after neoadjuvant Aumolertinib treatment. In contrast, Ex21-L858R samples after neoadjuvant Aumolertinib treatment showed upregulation in pathways related to “cell cycle transition, DNA replication, and cytoskeletal reconstruction” (Fig. 4j). Immune infiltration analysis revealed that post-treatment Ex19-Del samples exhibited significantly higher immune cell infiltration compared to Ex21-L858R samples, particularly in CD8 + T-cells, myeloid dendritic cells, and macrophages/monocytes (Fig. 4k). Moreover, the marker for alveolar macrophages, PPARG, was also upregulated (Supplementary Fig. 3i). Alveolar macrophages generally function in the cleanup and tissue repair process when there is extensive tumor cell necrosis³³. Previous research reports that MAPK pathway activation is correlated with Osimertinib resistance³⁴. Consistently, PROGNEY analysis showed a significant decrease in the MAPK pathway in Ex19-Del samples but not in Ex21-L858R samples after neoadjuvant Aumolertinib treatment (Fig. 4l). It is reported that the efficacy of immunotherapy was



positively associated with defective DNA mismatch repair (dMMR)³⁵. The dMMR was notably occurred in Ex19-Del samples, as well as other DNA repair mechanisms, including Nucleotide Excision Repair²³, Homology-dependent Recombination (HDR), and Non-homologous End Joining (NHEJ), which were potentially associated with the better responsive rate in Ex19-Del subgroup (Fig. 4I).

Discussion

Several prospective clinical trials and retrospective studies have explored the feasibility of neoadjuvant target-therapy for locally advanced NSCLC harboring driver gene mutation³⁶. However, EGFR-TKIs target-therapy has limited effect in improving the MPR rate and OS in NSCLCm compared to neoadjuvant chemotherapy. Recently

Fig. 4 | The changes of transcriptomic features and immune cell infiltration between pre-treatment and post-treatment tumor samples, and between Ex19-Del and Ex21-L858R tumor samples. a Clinical information related to all Aumolertinib cohort samples. **b** Differential gene expression between pre-treatment and post-treatment group in response samples, with immune-related genes marked in green. **c** GSEA results for upregulated pathways in the post-treatment response group. **d** Heatmap of MCPcounter scores, CIBERSORT scores, cytotoxicity, and HLA molecule expression for all samples (* indicates statistical significance between the pre-treatment group and the post-treatment group within response samples). **e** Alterations in TME classifications across the pre-treatment non-response, post-treatment non-response, pre-treatment response, and post-treatment response groups. **f** Variations in PD-1 and PD-L1 expression levels between the pre-treatment group and post-treatment group within response samples. Statistical comparisons were performed using one-sided Wilcoxon tests (left: $p = 0.01$; right: $p = 0.30$). **g** Variations in CCL2 and IL10 expression levels between the pre-treatment group and post-treatment group within response samples. Statistical comparisons were performed using one-sided Wilcoxon tests (left: $p = 0.43$; right: $p = 0.33$). **h** Variations in immune infiltration profiles between the Ex19-Del group and the Ex21-L858R group in the OncoSG Cohort. (two-sided Wilcoxon tests: T cell, $p = 0.30$; CD8 + T cell, $p = 0.60$; B cell, $p = 0.12$; NK cell, $p = 0.72$; macrophage/

monocyte, $p = 0.40$; myeloid dendritic cell, $p = 0.74$). **i** Differential gene expression between the Ex21-L858R group and the Ex19-Del group in post-treatment response samples, with distinct gene categories highlighted in various colors. **j** GSEA outcomes for the Ex21-L858R group and the Ex19-Del group in post-treatment response samples. **k** Immune infiltration differences between the Ex19-Del group and the Ex21-L858R group within the post-treatment response samples (values represent relative changes calculated by subtracting each group's pre-treatment mean from their post-treatment response values) (one-sided Wilcoxon tests: T cell, $p = 0.07$; CD8 + T cell, $p = 0.01$; B cells, $p = 0.14$; NK cell, $p = 0.14$; macrophage/monocyte, $p = 0.005$; myeloid dendritic cell, $p = 0.03$). **l** Heatmap of PROGENY scores and GSVA scores for DNA repair-related pathways across all samples (* indicates statistical significance between the Ex19-Del group and the Ex21-L858R group within the post-treatment response samples). Centers, boxes, whiskers, and dots indicate medians, quantiles, minima/maxima, and outliers, respectively. NS: $p \geq 0.05$; *: $0.01 \leq p < 0.05$; **: $0.001 \leq p < 0.01$; BER: Base Excision Repair; NER: Nucleotide Excision Repair; MMR: Mismatch Repair; HDR: Homology-dependent recombination; NHEJ: Non-homologous End Joining; DR: Direct Repair; TLS: Translesion Synthesis; NP: Nucleotide pools. Source data are provided as a Source Data file.

published studies have demonstrated that neoadjuvant Osimertinib (a third-generation *EGFR*-TKI) results in better ORR than the first-generation *EGFR*-TKIs and traditional chemotherapy in operable locally advanced NSCLCm, though it has not improved the MPR rate as anticipated^{10,12}. This phase II prospective trial attempts to assess the feasibility of neoadjuvant Aumolertinib treatment for unresectable locally advanced NSCLCm. The results demonstrate that neoadjuvant Aumolertinib achieves a favorable ORR (36/51, 70.6%), and has an acceptable toxicity profile. Furthermore, more than 40% of unresectable stage III NSCLCm patients (23/51, 45.1%) were converted into resectable status after neoadjuvant Aumolertinib treatment.

The trial achieved the pre-specified primary endpoint (ORR: 70.6%), which has potential advantages over the published results of clinical trials previously. This phenomenon might be caused by the following reasons. Firstly, the third-generation *EGFR*-TKIs have demonstrated significantly higher ORR compared to the first-generation *EGFR*-TKIs and traditional chemotherapy for NSCLCm in advanced stage^{7,37,38}. This suggests that the third-generation *EGFR*-TKIs might be more effective in creating opportunities for radical resection in patients with unresectable NSCLCm. Secondly, the number of neoadjuvant treatment cycles is a crucial issue for unresectable stage III patients. This trial was designed for initial unresectable stage III participants to receive neoadjuvant target-therapy for 16 weeks, which was significantly longer than other studies^{10,12}. However, prolonging the duration of neoadjuvant therapy might improve the incidence of *EGFR*-TKIs resistance and the difficulty of surgical resection potentially. Thus, the optimal number of therapeutic cycles requires further discussion. In this trial, 19 participants (37.3%, 19/51) received radical surgery after neoadjuvant therapy for no more than 4 cycles (only one participant received 3 cycles neoadjuvant therapy). Extending neoadjuvant treatment cycle created an opportunity for radical surgery in four participants (12.5%, 4/32). The potential impact of prolonging neoadjuvant therapy on enhancing the surgical conversion rate among patients with initially unresectable conditions remains an area requiring further investigation. Furthermore, the value of salvage surgery for NSCLCm patients who remain inoperable after neoadjuvant therapy remains controversial, necessitating further investigation³⁹.

Based on previous clinical experiences, NSCLC harboring Ex19-Del and Ex21-L858R mutations can be considered distinct due to their different responses to *EGFR*-TKIs^{11,40}. In this trial, comparing participants with Ex21-L858R mutation, Ex19-Del mutant participants have significantly higher ORR on radiological evaluation (91% vs 59%, $p = 0.006$), and significantly lower mean percentage of residual tumor cells on pathological evaluation (19.8% vs 63.5%, $p = 0.015$) after

neoadjuvant Aumolertinib treatment. In addition, achieving MPR after neoadjuvant treatment is a crucial prognostic factor for locally advanced NSCLC. The results of this trial demonstrate that Aumolertinib may be more effective for patients with Ex19-Del mutation. However, the relatively low MPR rate for NSCLCm indicates that *EGFR*-TKIs have limited efficacy in curing NSCLCm. Consequently, improving the prognosis of NSCLCm, particularly those with Ex21-L858R mutation remains a crucial issue and an area of significant concern.

In the above context, the results of bulk RNA-seq in this trial demonstrates that Ex21-L858R samples demonstrate a more extensive expression of cell cycle activation-related genes and pathways comparing to Ex19-Del samples. This finding aligns with the research of Zhu et al., which demonstrated that, relative to the L858R mutation, Ex19-Del cells showed enhanced suppression of AKT/ERK phosphorylation and G1 phase arrest upon Gefitinib treatment⁴¹ correlating with improved long-term survival in Ex19-Del patients. Our results extend this paradigm by identifying FBXO43-mediated⁴² stabilization of SKP2⁴³ as a novel mechanism facilitating cell cycle progression in Ex21-L858R tumor cells following TKI treatment. Specifically, FBXO43 is upregulated in post-treatment Ex21-L858R samples, where AT1 phosphorylation diminishes SKP2 ubiquitination and degradation. SKP2, a known oncogene, facilitates the ubiquitination and subsequent degradation of tumor suppressor substrates. Additionally, we observed an upregulation of the MAPK pathway, which is critically linked to *EGFR*-TKI resistance in patients harboring the Ex21-L858R mutation treated with *EGFR*-TKIs³⁴. The differential activation of the cell cycle and MAPK pathways between these two mutant subtypes may constrain the therapeutic efficacy of neoadjuvant Aumolertinib treatment in Ex21-L858R mutation patients.

Moreover, our study uncovers previously unreported immunological differences between the two mutation subtypes: Ex19-Del tumors demonstrate a higher degree of post-TKI immune activation, characterized by elevated CD8 + T cell/myeloid dendritic cell populations, and an upregulation of dMMR compared to Ex21-L858R tumors. This novel finding contrasts with Zhu et al.'s focus on cell-autonomous signaling, and suggests that the superior clinical outcomes observed in Ex19-Del patients may stem from intrinsic signaling vulnerabilities and immune permissiveness. The concurrent upregulation of NER/HDR/NHEJ DNA repair pathways in Ex19-Del tumors further points to a distinct adaptive DNA repair mechanism that could potentially enhance the efficacy of subsequent immunotherapy³⁵, a therapeutic approach not previously considered in studies comparing *EGFR* mutation subtypes. These insights imply that Ex21-L858R patients may benefit from the earlier incorporation of cell cycle/MAPK inhibitors alongside TKIs,

whereas Ex19-Del tumors may derive greater benefit from sequential immunotherapy.

As the frontline therapeutic agents for patients with *EGFR* mutations, *EGFR*-TKIs induce dynamic alterations in TME, and the implications of these changes for subsequent immunotherapy remain a matter of debate^{44–47}. Our results from bulk RNA-Seq have elucidated that in patients exhibiting a response to Aumolertinib, there is an upregulation of genes such as IL2, LAT, and KLRK1, which are integral to the proliferation and activation of T cells and NK cells. We also observed an enhancement in lymphocyte, leukocyte, and NK cell-mediated immune pathways. Immune infiltration analysis confirms a notable increase in CD8⁺ T cells, NK cells, and myeloid dendritic cells post-treatment. Concurrently, cytotoxic molecules and HLA are also elevated, which are closely associated with CD8⁺ T cells, corroborating the findings of Lu et al., who demonstrated that short-term TKI treatment enhances antitumor immunity by promoting the infiltration of cytotoxic cells⁴⁸. Furthermore, our classification of TME in tumor samples identified a significant upregulation in the Immune-Enriched-Non-Fibrotic subtype, which is most conducive to immunotherapy, following neoadjuvant *EGFR*-TKIs treatment. Interestingly, PD-1 expression in primary tumors is markedly increased after neoadjuvant *EGFR*-TKIs treatment. However, between baseline and post-treatment tumor samples, a similar trend could not be observed in PD-L1 expression, especially in the non-response group^{49,50}. Taken together, our observation continues to suggest the potential effectiveness of a sequential treatment regimen involving *EGFR*-TKIs followed by immunotherapy, particularly in patients with Ex19-Del mutations. By strategically implementing immunotherapy during the period when *EGFR*-TKIs induce tumor microenvironment activation, it may be feasible to achieve maximal remission for inoperable stage III NSCLCm patients.

Several limitations are present in this trial. First, the neoadjuvant therapeutic efficacy of Aumolertinib could not be directly compared with other regimens due to the single-arm design. Second, the relatively small sample size of this phase II trial may limit the robustness of the evidence regarding therapeutic efficacy. Third, the choice of adjuvant treatment regimens for stage III NSCLCm remains controversial and may influence the participants' prognosis. Fourth, the relatively short follow-up period prevents establishing a definitive correlation between the primary endpoint and long-term survival outcomes. These limitations suggest that the efficacy of neoadjuvant *EGFR*-TKIs requires long-term follow-up and more relevant participants to validate. Fifth, the bulk RNA-seq analysis lacked paired tumor samples, and future studies should prioritize the collection of paired samples to enable more robust longitudinal analyses. Furthermore, our study faces challenges common to clinical trials of *EGFR*-TKIs (such as FLAURA2⁵¹ and ARCHER 1050⁵²), where the limited availability of tissue samples in real-world clinical settings hinders the ability to perform multi-omics analyses. Although our bulk RNA-seq data revealed patterns of immune activation, spatial transcriptomics, which maps gene expression within the tissue architecture, could more precisely elucidate the local immune microenvironment and tumor-stroma interactions. In the future, it will be necessary to integrate spatial analysis into single-cell or multi-region sequencing to validate our findings and further dissect the spatial determinants of treatment response. Given the constraints in sample size and the dimensionality of omics data, cautious interpretation is advised. Future research should employ multi-temporal sampling and incorporate multi-omics approaches to more robustly validate these findings.

In conclusion, neoadjuvant Aumolertinib treatment maintains an acceptable toxicity profile for stage III *EGFR*-mutant NSCLC. Besides, this treatment also offers a favorable objective tumor response for these patients, especially for Ex19-Del mutant patients. The dynamic alterations observed in the TME, particularly in

responsive patients and those with the Ex19-Del mutation, offer valuable insights. These findings may help identify predictive biomarkers for target-therapy and guide the design and focus of future clinical trials.

Methods

Study design

This single-arm phase II trial was conducted at Shanghai Pulmonary Hospital, which was registered at <https://www.clinicaltrials.gov> before participant enrollment (NCT04685070). The study was approved by the independent ethic committee in Shanghai Pulmonary Hospital (L20-427), and conducted in accordance with the Declaration of Helsinki (as revised in 2013). Informed consents were obtained from all participants. The study protocol is provided in the Supplementary Information file.

Patient eligibility

Treatment naive inoperable stage III NSCLCm⁵³, older than 18 years, with an Eastern Cooperative Oncology Group (ECOG) performance status of 0 or 1, were enrolled in this trial between December 14th, 2021 and June 15th, 2023. The diagnosis of NSCLC was confirmed by immunohistochemical detections by endobronchial ultrasound (EBUS) or percutaneous lung biopsy. *EGFR*-mutant status was diagnosed by polymerase chain reaction. The clinical staging was confirmed by chest computed tomography (CT), and brain magnetic resonance imaging (MRI), positron emission tomography/computed tomography (PET/CT). Patients were required to have normal hematological indexes, qualified hepatic, renal, and pulmonary functions so that neoadjuvant therapy followed by radical resection could be tolerated.

A detailed definition of inoperable stage III NSCLC was provided in a previously published clinical trial in our center (LungMate 003, NCT04379739⁵³), and was updated in this study. The inoperable stage III NSCLCm meet the following characteristics and might be performed radical resection after neoadjuvant target-therapy. First: the primary tumor or metastatic lymph nodes invading vital structures (large blood vessels, trachea, primary bronchus). Second: mediastinal lymph nodes (N2) with multi-station metastasis or bulky fusion. Third: mediastinal lymph nodes (N3) metastasis. Fourth: R0 resection may not be achieved, even if pneumonectomy was performed according to preoperative evaluation.

Pregnant or breast-feeding patients, patients with unstable systemic disease (interstitial lung disease, pulmonary fibrosis, cardiovascular disease and so on), patients with any anticancer therapy outside of this trial (*EGFR*-TKIs, chemotherapies, immunotherapies, and so on) were ineligible for this trial.

Procedures

Participants received 16 weeks (4 cycles) administration of Aumolertinib (Hansoh Pharmaceutical Group Co, Ltd, Shanghai, China) (Aumolertinib 110 mg, oral, once-daily). Chest CT were performed at the 8th and 16th weeks after treatment or before surgical treatment. All CT scans of participants were assessed by the same radiologist and 3 experienced thoracic surgeons via Response Evaluation Criteria in Solid Tumors measurement criteria (RECIST, version 1.1). Radiologically partial response²¹ or responder were defined as at least a 30% decrease in the sum of TLD versus baseline. If participants after neoadjuvant treatment could be resected completely, surgery could be performed within two weeks after Aumolertinib discontinuation. Adjuvant Aumolertinib treatment could be administrated within eight weeks postoperatively. We strongly recommend that the participants continue long-term adjuvant therapy for at least three years or until the disease progresses. However, if participants were still inoperable after 16 weeks neoadjuvant treatment, they should be treated based on multi-disciplinary therapy (MDT).

Efficacy and safety assessment

The primary endpoint was ORR assessed by the RECIST (version 1.1). The secondary endpoints were MPR and pCR rate in radical surgery treated participants, EFS, OS, and TRAEs in all participants.

Sample size estimation

The primary endpoint of this research was ORR, which was taken to calculate the sample size. Meta analysis calculated that the ORR of neoadjuvant the first-generation *EGFR*-TKIs for locally advanced NSCLC in previous studies (EMERGING-CTONG 1103⁵⁴) was 52%. The ORR of Aumolertinib for advanced NSCLC (APOLLO⁵⁵) was 68.9%. Therefore, the ORR was expected to be 70% in this trial, and the neoadjuvant the first-generation *EGFR*-TKIs was taken as the historical control group. It was calculated with $\alpha = 0.05$ (one-tailed⁸) and the power of test ($1 - \beta$) = 80%. The sample size will be 45 as calculated. With a drop-off rate of 20%, the total sample size will be 56.

&: If the null hypothesis of the statistical test is that the ORR of drug A is superior to that of drug B, only one scenario needs to be considered, rendering a one-sided test adequate to fulfill the statistical requirements. In this trial, our objective is solely to investigate whether the ORR of third-generation TKIs in neoadjuvant settings exceeds that of first-generation TKIs.

Follow-up

Follow-up was achieved by outpatient visit or telephone contact. For surgical treated participants, chest CT were performed every 3 months for the first year postoperatively, every 6 months for 2 to 5 years, and annually from then on. MRI of the brain, ultrasonography of abdominal regions, bone scans were performed annually. The follow-up was conducted until death. Local recurrence was defined as the recurrence in the primary site or mediastinal lymph nodes, while distant recurrence was defined as recurrence in other sites.

RNA sequencing and data processing

Total RNA was extracted from fresh-frozen tissue using TRIzol. The sequencing library was prepared using the NEBNext Ultra RNA Library Prep Kit for Illumina and indexed to facilitate sample-specific sequence assignment. After library preparation, the libraries were pooled and subjected to paired-end sequencing (2×150 bp reads) on an Illumina NovaSeq 6000 platform. Following RNA sequencing, the raw FASTQ files were trimmed using fastp (v0.23.4)⁵⁶ and aligned to the GRCh38 reference genome using STAR (v2.7.9a)⁵⁷ with default settings. After obtaining BAM files, read counts were summarized using featureCounts (v2.0.6)⁵⁸ and TPM (Transcripts Per Million) values were generated using Salmon (v0.14.1)⁵⁹.

Differentially expressed gene analysis

Differential gene expression between sample groups was assessed using DESeq2⁶⁰. DESeq2 models gene count expression data and computes log2 fold changes, which estimate effect sizes and represent gene variations between comparison groups. Two-sided Wald test statistics were calculated to examine differential expression between the groups. Genes with $|\text{Log}_2 \text{ Fold Change}| > 1$ and Wald test $p < 0.05$ were defined as differentially expressed genes. The differential genes expression results were visualized by the volcano plots.

Gene set enrichment analysis (GSEA) and gene set variation analysis (GSVA)

Enrichment analysis was performed using GSEA⁶¹ and GSVA⁶². In GSEA analysis, results for all protein-coding genes were ranked by log2 fold change and evaluated using GSEA algorithm. Gene sets related to Gene Ontology Biological Processes (GOBP) were obtained from MSigDb. GSEA results were filtered based on a $p < 0.05$, and pathways were visualized as candidate pathways according to their normalized enrichment scores. For GSVA, gene expression distribution densities

were calculated for each gene set across all samples. The overall expression distribution of each gene set in a sample was obtained by integrating the expression distribution densities of all genes within the gene set. Relative scores were computed by comparing the density distributions of genes within the gene set to the density distributions of background genes.

Tumor microenvironment assessment

Immune cell infiltration was assessed using MCPCounter (v1.1.0), CIBERSORT (v1.01), Quantiseq (v1.10.0)²³, and TIMER2²⁴. Tumor samples were classified into four microenvironment subtypes (depleted, fibrotic, immune-enriched-nonfibrotic and immune-enriched-fibrotic) using molecular functional profiles as defined by Bagaev²⁵. Malignant pathways were assessed using PROGENy.

Statistical analysis

Efficacy and safety analyses were based on the intention-to-treat (ITT) population who received neoadjuvant treatment at least one dose. While, pathological efficacies were evaluated by participants who received neoadjuvant treatment followed by surgery. Descriptive statistics, chi-squares test, Fisher's exact test, independent sample *t*-test, matched sample *t*-test, Kaplan-Meier method, and Log-Rank test were used. The median follow-up time was calculated by reverse Kaplan-Meier method. EFS and OS were calculated and reported in this work to evaluate the feasibility of neoadjuvant treatment. EFS was defined as the time between the first dosage of neoadjuvant Aumolertinib and any progression of disease before surgery, disease recurrence after surgery, disease progression in the absence of surgery, treatment strategy changing from any reasons, or death from any cause. If the participants of this trial have several of the above events in turn during the follow-up period, the first event during the follow-up period is defined as the event related to "event-free survival (EFS)". OS was defined as the first dosage of neoadjuvant Aumolertinib to death from any cause. The Wilcoxon rank sum test was utilized to independently assess the differences between the sample groups. For the clinical analysis, *p*-values were calculated using a two-sided method. Conversely, in the bioinformatics analysis, due to the limited sample size, a one-sided method was employed. Statistical significance was determined by a threshold of $p < 0.05$ in both contexts. Clinical information of participants enrolled in this trial was recorded in case report form (CRF) in paper version. Clinical data were analyzed by SPSS software (version 26.0, IBM Corp, Armonk, NY), and exploratory analyses were conducted using R programming (version 4.2.0).

Reporting summary

Further information on research design is available in the Nature Portfolio Reporting Summary linked to this article.

Data availability

The protocol of this trial is available in the Supplementary Information as a Supplementary Note. The OncoSG cohort data used in this study is publicly accessible through the OncoSG database (<https://src.gisapps.org/OncoSG/>) under accession number GIS031. The original RNA sequencing data have been archived in the Genome Sequence Archive at the National Genomics Data Center, under accession number HRA008462. In accordance with the People's Republic of China's regulations on human genetic resources, patient clinical data have been anonymized. Access to the dataset is controlled, requiring researchers to submit a formal application to the Data Access Committee (DAC) detailing their research objectives and ethical compliance. Upon approval, access will be granted for 6 months to 2 years, and the data will be available to designated research accounts. All remaining data can be found in the Article, Supplementary and Source Data files. Source data are provided with this paper.

Code availability

While no novel algorithms were introduced in this study, all code employed during the experiments is available from the corresponding authors upon request for research purposes, thereby ensuring both transparency and reproducibility.

References

- Goldstraw, P. et al. The IASLC Lung Cancer Staging Project: Proposals for Revision of the TNM Stage Groupings in the Forthcoming (Eighth) Edition of the TNM Classification for Lung Cancer. *J. Thorac. Oncol.* **11**, 39–51 (2016).
- Arbour, K. C. & Riely, G. J. Systemic Therapy for Locally Advanced and Metastatic Non-Small Cell Lung Cancer: A Review. *Jama.* **322**, 764–774 (2019).
- Zhao, Y. et al. Efficacy and safety of first line treatments for patients with advanced epidermal growth factor receptor mutated, non-small cell lung cancer: systematic review and network meta-analysis. *BMJ.* **367**, 15460 (2019).
- Spigel, D. R. et al. Five-Year Survival Outcomes From the PACIFIC Trial: Durvalumab After Chemoradiotherapy in Stage III Non-Small-Cell Lung Cancer. *J. Clin. Oncol.* **40**, 1301–1311 (2022).
- Zhou, Q. et al. Sugemalimab versus placebo after concurrent or sequential chemoradiotherapy in patients with locally advanced, unresectable, stage III non-small-cell lung cancer in China (GEMSTONE-301): interim results of a randomised, double-blind, multicentre, phase 3 trial. *Lancet Oncol.* **23**, 209–219 (2022).
- Girard, N. et al. Treatment Characteristics and Real-World Progression-Free Survival in Patients With Unresectable Stage III NSCLC Who Received Durvalumab After Chemoradiotherapy: Findings From the PACIFIC-R Study. *J. Thorac. Oncol.* **18**, 181–193 (2023).
- Lu, S. et al. AENEAS: A Randomized Phase III Trial of Aumolertinib Versus Gefitinib as First-Line Therapy for Locally Advanced or Metastatic Non-Small-Cell Lung Cancer With EGFR Exon 19 Deletion or L858R Mutations. *J. Clin. Oncol.* **40**, 3162–3171 (2022).
- Lu, S. et al. Osimertinib after Chemoradiotherapy in Stage III EGFR-Mutated NSCLC. *N. Engl. J. Med.* **391**, 585–597 (2024).
- Wu, Y. L. et al. Osimertinib in Resected EGFR-Mutated Non-Small-Cell Lung Cancer. *N. Engl. J. Med.* **383**, 1711–1723 (2020).
- Blakely, C. M. et al. Neoadjuvant Osimertinib for the Treatment of Stage I-IIIa Epidermal Growth Factor Receptor-Mutated Non-Small Cell Lung Cancer: A Phase II Multicenter Study. *J. Clin. Oncol.* **42**, 3105–3114 (2024).
- Bian, D. et al. Neoadjuvant Afatinib for stage III EGFR-mutant non-small cell lung cancer: a phase II study. *Nat. Commun.* **14**, 4655 (2023).
- Lv, C. et al. Osimertinib as neoadjuvant therapy in patients with EGFR-mutant resectable stage II-IIIB lung adenocarcinoma (NEOS): A multicenter, single-arm, open-label phase 2b trial. *Lung Cancer* **178**, 151–156 (2023).
- Zhong, W. Z. et al. Erlotinib versus gemcitabine plus cisplatin as neoadjuvant treatment of stage IIIA-N2 EGFR-mutant non-small-cell lung cancer: final overall survival analysis of the EMERGING-CTONG 1103 randomised phase II trial. *Signal Transduct. Target Ther.* **8**, 76 (2023).
- Lee, J. B. et al. Neoadjuvant and adjuvant osimertinib in stage IA-IIIa, EGFR-mutant non-small cell lung cancer (NORA). *J. Thorac Oncol.* **24**, 02544-9 (2024).
- Shirley, M. & Kearn, S. J. Aumolertinib: A Review in Non-Small Cell Lung Cancer. *Drugs* **82**, 577–584 (2022).
- Feng, S. et al. Case Report: Aumolertinib as Neoadjuvant Therapy for Patients With Unresectable Stage III Non-Small Cell Lung Cancer With Activated EGFR Mutation: Case Series. *Front Oncol.* **12**, 872225 (2022).
- Zhu, L. et al. Thoracic radiotherapy and concurrent almonertinib for unresectable stage III EGFR-mutated non-small-cell lung cancer: a phase 2 study. *BMC Cancer* **21**, 511 (2021).
- Wu, J. et al. An activating immunoreceptor complex formed by NKG2D and DAP10. *Science* **285**, 730–732 (1999).
- Mingari, M. C. et al. Human interleukin-2 promotes proliferation of activated B cells via surface receptors similar to those of activated T cells. *Nature* **312**, 641–643 (1984).
- Yang, Y. et al. The Us3 Protein of Herpes Simplex Virus 1 Inhibits T Cell Signaling by Confining Linker for Activation of T Cells (LAT) Activation via TRAF6 Protein. *J. Biol. Chem.* **290**, 15670–15678 (2015).
- Becht, E. et al. Estimating the population abundance of tissue-infiltrating immune and stromal cell populations using gene expression. *Genome Biol.* **17**, 218 (2016).
- Newman, A. M. et al. Robust enumeration of cell subsets from tissue expression profiles. *Nat. Methods* **12**, 453–457 (2015).
- Finotello, F. et al. Molecular and pharmacological modulators of the tumor immune contexture revealed by deconvolution of RNA-seq data. *Genome Med.* **11**, 34 (2019).
- Li, T. et al. TIMER2.0 for analysis of tumor-infiltrating immune cells. *Nucleic Acids Res.* **48**, W509–w514 (2020).
- Bagaev, A. et al. Conserved pan-cancer microenvironment subtypes predict response to immunotherapy. *Cancer Cell* **39**, 845–865.e847 (2021).
- Jia, Y. et al. EGFR-targeted therapy alters the tumor microenvironment in EGFR-driven lung tumors: Implications for combination therapies. *Int J. Cancer* **145**, 1432–1444 (2019).
- Osipov, A., Saung, M. T., Zheng, L. & Murphy, A. G. Small molecule immunomodulation: the tumor microenvironment and overcoming immune escape. *J. Immunother. Cancer* **7**, 224 (2019).
- Chen, J. et al. Genomic landscape of lung adenocarcinoma in East Asians. *Nat. Genet.* **52**, 177–186 (2020).
- Yang, R. et al. E2F7-EZH2 axis regulates PTEN/AKT/mTOR signalling and glioblastoma progression. *Br. J. Cancer* **123**, 1445–1455 (2020).
- Arora, S. et al. Unravelling the Role of miR-20b-5p, CCNB1, HMGA2 and E2F7 in Development and Progression of Non-Small Cell Lung Cancer (NSCLC). *Biology (Basel)* **9**, 201 (2020).
- Novak, D. et al. SOX2 in development and cancer biology. *Semin Cancer Biol.* **67**, 74–82 (2020).
- Gao, Y. et al. LncRNA PCAT1 activates SOX2 and suppresses radioimmune responses via regulating cGAS/STING signalling in non-small cell lung cancer. *Clin. Transl. Med.* **12**, e792 (2022).
- Pervizaj-Oruqaj, L., Ferrero, M. R., Matt, U. & Herold, S. The guardians of pulmonary harmony: alveolar macrophages orchestrating the symphony of lung inflammation and tissue homeostasis. *Eur. Respir. Rev.* **33**, 230263 (2024).
- Eberlein, C. A. et al. Acquired Resistance to the Mutant-Selective EGFR Inhibitor AZD9291 Is Associated with Increased Dependence on RAS Signaling in Preclinical Models. *Cancer Res.* **75**, 2489–2500 (2015).
- Luchini, C. et al. ESMO recommendations on microsatellite instability testing for immunotherapy in cancer, and its relationship with PD-1/PD-L1 expression and tumour mutational burden: a systematic review-based approach. *Ann. Oncol.* **30**, 1232–1243 (2019).
- Yu, Z., Xu, F. & Zou, J. Feasibility and safety of EGFR-TKI neoadjuvant therapy for EGFR-mutated NSCLC: A meta-analysis. *Eur. J. Clin. Pharmacol.* **80**, 505–517 (2024).
- Soria, J. C. et al. Osimertinib in Untreated EGFR-Mutated Advanced Non-Small-Cell Lung Cancer. *N. Engl. J. Med.* **378**, 113–125 (2018).
- Shi, Y. et al. Furmonertinib (AST2818) versus gefitinib as first-line therapy for Chinese patients with locally advanced or metastatic EGFR mutation-positive non-small-cell lung cancer (FURLONG): a

- multicentre, double-blind, randomised phase 3 study. *Lancet Respir. Medicine*. **10**, 1019–1028 (2022).
39. Andrews, W. G. et al. Persistent N2 After Induction Is Not a Contraindication to Surgery for Lung Cancer. *Ann. Thorac. Surg.* **114**, 394–400 (2022).
 40. Sequist, L. V. et al. Phase III study of afatinib or cisplatin plus pemetrexed in patients with metastatic lung adenocarcinoma with EGFR mutations. *J. Clin. Oncol.* **31**, 3327–3334 (2013).
 41. Zhu, J. Q. et al. Better survival with EGFR exon 19 than exon 21 mutations in gefitinib-treated non-small cell lung cancer patients is due to differential inhibition of downstream signals. *Cancer Lett.* **265**, 307–317 (2008).
 42. Zheng, L. et al. FBXO43 promotes cell cycle progression in cancer cells through stabilizing SKP2. *Cancer Lett.* **591**, 216848 (2024).
 43. Carrano, A. C., Eytan, E., Hershko, A. & Pagano, M. SKP2 is required for ubiquitin-mediated degradation of the CDK inhibitor p27. *Nat. Cell Biol.* **1**, 193–199 (1999).
 44. Zhao, Y. et al. AK112, a novel PD-1/VEGF bispecific antibody, in combination with chemotherapy in patients with advanced non-small cell lung cancer (NSCLC): an open-label, multicenter, phase II trial. *EClinicalMedicine* **62**, 102106 (2023).
 45. Lu, S. et al. Sintilimab plus chemotherapy for patients with EGFR-mutated non-squamous non-small-cell lung cancer with disease progression after EGFR tyrosine-kinase inhibitor therapy (ORIENT-31): second interim analysis from a double-blind, randomised, placebo-controlled, phase 3 trial. *Lancet Respir. Med.* **11**, 624–636 (2023).
 46. Nogami, N. et al. IMpower150 Final Exploratory Analyses for Atezolizumab Plus Bevacizumab and Chemotherapy in Key NSCLC Patient Subgroups With EGFR Mutations or Metastases in the Liver or Brain. *J. Thorac. Oncol.* **17**, 309–323 (2022).
 47. Isomoto, K. et al. Impact of EGFR-TKI Treatment on the Tumor Immune Microenvironment in EGFR Mutation-Positive Non-Small Cell Lung Cancer. *Clin. Cancer Res.* **26**, 2037–2046 (2020).
 48. Lu, C. et al. Understanding the dynamics of TKI-induced changes in the tumor immune microenvironment for improved therapeutic effect. *J. Immunother Cancer* **12**, e009165 (2024).
 49. Yang, J. C. et al. Pembrolizumab in Combination With Erlotinib or Gefitinib as First-Line Therapy for Advanced NSCLC With Sensitizing EGFR Mutation. *J. Thorac. Oncol.* **14**, 553–559 (2019).
 50. Tang, Y. et al. The association between PD-L1 and EGFR status and the prognostic value of PD-L1 in advanced non-small cell lung cancer patients treated with EGFR-TKIs. *Oncotarget* **6**, 14209–14219 (2015).
 51. Planchard, D. et al. Osimertinib with or without Chemotherapy in EGFR-Mutated Advanced NSCLC. *N. Engl. J. Med.* **389**, 1935–1948 (2023).
 52. Cheng, Y. et al. Safety and efficacy of first-line dacomitinib in Asian patients with EGFR mutation-positive non-small cell lung cancer: Results from a randomized, open-label, phase 3 trial (ARCHER 1050). *Lung Cancer* **154**, 176–185 (2021).
 53. Xia, H. et al. Neoadjuvant camrelizumab (an anti-PD-1 antibody) plus chemotherapy or apatinib (a VEGFR-2 inhibitor) for initially unresectable stage II-III non-small-cell lung cancer: a multicentre, two-arm, phase 2 exploratory study. *Signal Transduct. Target Ther.* **9**, 145 (2024).
 54. Zhong, W. et al. EGFRerlotinib Versus Gemcitabine Plus Cisplatin as Neoadjuvant Treatment of Stage IIIA-N2 -Mutant Non-Small-Cell Lung Cancer (EMERGING-CTONG 1103): A Randomized Phase II Study. *J. Clin. Oncol.: Off. J. Am. Soc. Clin. Oncol.* **37**, 2235–2245 (2019).
 55. Lu, S. et al. Efficacy of Aumolertinib (HS-10296) in Patients With Advanced EGFR T790M+ NSCLC: Updated Post-National Medical Products Administration Approval Results From the APOLLO Registrational Trial. *J. Thorac. Oncol.* **17**, 411–422 (2022).
 56. Chen, S. Ultrafast one-pass FASTQ data preprocessing, quality control, and deduplication using fastp. *Imeta* **2**, e107 (2023).
 57. Dobin, A. et al. STAR: ultrafast universal RNA-seq aligner. *Bioinformatics* **29**, 15–21 (2013).
 58. Liao, Y., Smyth, G. K. & Shi, W. featureCounts: an efficient general purpose program for assigning sequence reads to genomic features. *Bioinformatics* **30**, 923–930 (2014).
 59. Patro, R., Duggal, G., Love, M. I., Irizarry, R. A. & Kingsford, C. Salmon provides fast and bias-aware quantification of transcript expression. *Nat. Methods* **14**, 417–419 (2017).
 60. Love, M. I., Huber, W. & Anders, S. Moderated estimation of fold change and dispersion for RNA-seq data with DESeq2. *Genome Biol.* **15**, 550 (2014).
 61. Subramanian, A. et al. Gene set enrichment analysis: a knowledge-based approach for interpreting genome-wide expression profiles. *Proc. Natl. Acad. Sci. USA* **102**, 15545–15550 (2005).
 62. Hänzelmann, S., Castelo, R. & Guinney, J. GSEA: gene set variation analysis for microarray and RNA-seq data. *BMC Bioinforma.* **14**, 7 (2013).

Acknowledgements

We thank all participants and their relatives for being a part of this trial. This work was supported by Hansoh Pharmaceutical Group Co, Ltd, Shanghai, China, National Natural Science Foundation of China (Grant No. 82430053, P.Z., 82125001, P.Z.), the Shanghai Science and Technology Committee (Grant No.24SF1904500, P.Z.), Innovation Program of Shanghai Municipal Education Commission (Grant No. 2023ZKZD33, P.Z.), foundation of Shanghai Pulmonary Hospital (Grant No. TJ-FK-YXJC003, P.Z., LYRC202402, P.Z., FKLY20004, P.Z.), and Shanghai Pulmonary Hospital “Elite Sail” Talent Program (Grant No. 2024FKJY2403, D.B.). The sponsor and funders had no role in study design, data collection, data analysis, or manuscript writing.

Author contributions

P.Z., and D.B. conceived and designed the study. L.J. M.L., W.H., L.D., D.X., X.L., Y.Zhu, X.Z., and J.Z. provided the materials and patients support. G.J., and D.Z. provided the administrative support. D.B., L.Z., C.W., Y.L., S.J., X.B., J.Y., Y.Zhou, Z.H., L.S., J.Hu., J.Huang, and J.L. collected the data. D.B., L.Z., Z.H., Y.L., S.J., L.S., J.Hu., and Y.Zheng. analyzed and interpreted the data. D.B., S.J., L.Z., and J.Hu. wrote the draft of the manuscript. All authors approved the final version of the manuscript for submission.

Competing interests

The authors declare no competing interests.

Additional information

Supplementary information The online version contains supplementary material available at <https://doi.org/10.1038/s41467-025-58435-9>.

Correspondence and requests for materials should be addressed to Chunyan Wu, Deping Zhao, Liang Duan, Gening Jiang or Peng Zhang.











Peer review information *Nature Communications* thanks Youdong Mao, Julien Marcoux and the other, anonymous, reviewer(s) for their contribution to the peer review of this work. A peer review file is available.

Reprints and permissions information is available at <http://www.nature.com/reprints>

Publisher’s note Springer Nature remains neutral with regard to jurisdictional claims in published maps and institutional affiliations.

Open Access This article is licensed under a Creative Commons Attribution-NonCommercial-NoDerivatives 4.0 International License, which permits any non-commercial use, sharing, distribution and reproduction in any medium or format, as long as you give appropriate credit to the original author(s) and the source, provide a link to the Creative Commons licence, and indicate if you modified the licensed material. You do not have permission under this licence to share adapted material derived from this article or parts of it. The images or other third party material in this article are included in the article's Creative Commons licence, unless indicated otherwise in a credit line to the material. If material is not included in the article's Creative Commons licence and your intended use is not permitted by statutory regulation or exceeds the permitted use, you will need to obtain permission directly from the copyright holder. To view a copy of this licence, visit <http://creativecommons.org/licenses/by-nc-nd/4.0/>.

© The Author(s) 2025

Dongliang Bian ^{1,9}, **Shuyu Ji**^{1,9}, **Yue Liu** ^{1,9}, **Zhida Huang**^{2,9}, **Lei Jiang**^{1,9}, **Ming Liu**^{1,9}, **Xiao Bao**^{3,9}, **Jie Yang**¹, **Yirui Zhou**¹, **Junjie Hu**¹, **Liangdong Sun**¹, **Yingzhi Zheng**¹, **Jie Huang**⁴, **Jing Liu**¹, **Xinsheng Zhu**¹, **Jing Zhang**¹, **Lele Zhang** ⁵, **Xiaogang Liu**¹, **Wenxin He** ¹, **Dong Xie**¹, **Yuming Zhu**¹, **Chunyan Wu**^{6,10} , **Deping Zhao**^{1,10} , **Liang Duan**^{1,10} , **Gening Jiang**^{1,10}  & **Peng Zhang** ^{1,7,8,10} 

¹Department of Thoracic Surgery, Shanghai Pulmonary Hospital, School of Medicine, Tongji University, Shanghai 200433, China. ²Department of Thoracic Surgery, Fujian Medical University Union Hospital, Fuzhou 350001, China. ³Department of Radiology, Shanghai Pulmonary Hospital, School of Medicine, Tongji University, Shanghai 200433, China. ⁴Department of Clinical Research Center, Shanghai Pulmonary Hospital, School of Medicine, Tongji University, Shanghai 200433, China. ⁵Department of Central Laboratory, Shanghai Pulmonary Hospital, School of Medicine, Tongji University, Shanghai 200433, China. ⁶Department of Pathology, Shanghai Pulmonary Hospital, School of Medicine, Tongji University, Shanghai 200433, China. ⁷Wenzhou Medical University, Wenzhou, Zhejiang 325035, China. ⁸Shihezi University School of Medicine, Shihezi, Xinjiang 832099, China. ⁹These authors contributed equally: Dongliang Bian, Shuyu Ji, Yue Liu, Zhida Huang, Lei Jiang, Ming Liu, Xiao Bao. ¹⁰These authors jointly supervised this work: Chunyan Wu, Deping Zhao, Liang Duan, Gening Jiang, Peng Zhang. ✉ e-mail: wuchunyan581@163.com; zdp1992@163.com; duan-liang@163.com; geningjiang@tongji.edu.cn; zhangpeng1121@tongji.edu.cn